DOI: 10.1104/pp.18.00709

The Patterned Structure of Galactoglucomannan Suggests It May Bind to Cellulose in Seed Mucilage[1][OPEN]

Li Yu,[a] Jan J. Lyczakowski,[a] Caroline S. Pereira,[b] Toshihisa Kotake,[a,c] Xiaolan Yu,[a] An Li,[a] Soren Mogelsvang,[a,2] Munir S. Skaf,[b] and Paul Dupree[a,3,4]

[a]Department of Biochemistry and The Leverhulme Trust Centre for Natural Material Innovation, University of Cambridge, Cambridge CB2 1QW, United Kingdom
[b]Institute of Chemistry, University of Campinas-UNICAMP, Campinas SP 13084-862, Brazil
[c]Division of Life Science, Graduate School of Science and Engineering, Saitama University, Saitama 338-8642, Japan

ORCID IDs: 0000-0001-8820-6705 (L.Y.); 0000-0002-7694-8629 (J.J.L.); 0000-0002-0248-0883 (C.S.P.); 0000-0002-1167-3273 (T.K.); 0000-0001-7415-8626 (S.M.); 0000-0001-7485-1228 (M.S.S.); 0000-0001-9270-6286 (P.D.)

The interaction between mannan polysaccharides and cellulose microfibrils contributes to cell wall properties in some vascular plants, but the molecular arrangement of mannan in the cell wall and the nature of the molecular bonding between mannan and cellulose remain unknown. Previous studies have shown that mannan is important in maintaining Arabidopsis (*Arabidopsis thaliana*) seed mucilage architecture, and that Cellulose Synthase-Like A2 (CSLA2) synthesizes a glucomannan backbone, which Mannan α-Galactosyl Transferase1 (MAGT1/GlycosylTransferase-Like6/Mucilage Related10) might decorate with single α-Gal branches. Here, we investigated the ratio and sequence of Man and Glc and the arrangement of Gal residues in Arabidopsis mucilage mannan using enzyme sequential digestion, carbohydrate gel electrophoresis, and mass spectrometry. We found that seed mucilage galactoglucomannan has a backbone consisting of the repeating disaccharide [4)-β-Glc-(1,4)-β-Man-(1,], and most of the Man residues in the backbone are substituted by single α-1,6-Gal. CSLA2 is responsible for the synthesis of this patterned glucomannan backbone and MAGT1 catalyses the addition of α-Gal. In vitro activity assays revealed that MAGT1 transferred α-Gal from UDP-Gal only to Man residues within the CSLA2 patterned glucomannan backbone acceptor. These results indicate that CSLAs and galactosyltransferases are able to make precisely defined galactoglucomannan structures. Molecular dynamics simulations suggested this patterned galactoglucomannan is able to bind stably to some hydrophilic faces and to hydrophobic faces of cellulose microfibrils. A specialization of the biosynthetic machinery to make galactoglucomannan with a patterned structure may therefore regulate the mode of binding of this hemicellulose to cellulose fibrils.

Plant cell walls are flexible yet relatively rigid polysaccharide-based structures that envelop the majority of plant cells. Cell walls influence the development and shape of plants, determine mechanical properties of plant tissues and organs, and impact cell-specific functions. The components of the plant cell wall constitute the most abundant element of plant biomass and, as such, offer a renewable source of carbohydrate for various industrial processes. However, the molecular architecture of the wall poses a challenge in the use of this material in industrial applications. Interactions between different polysaccharides and phenolic compounds constituting the cell wall form the basis of its molecular architecture. These interactions are fundamental to the properties of timber used in building construction. It is also important to understand how the components of the cell wall interact to develop more efficient use of the biomass in the paper, pulp, textile, and food industries and also to facilitate improvements in production of lignocellulosic biofuels.

Mannans consist of a linear backbone of β-1,4-linked residues of either Man or a combination of Glc and Man (Scheller and Ulvskov, 2010). Mannans have often been studied due to their role as seed storage compounds, but they are found in variable amounts in all plant cell walls (Moreira and Filho, 2008). The mannan backbone is composed entirely of Man in endosperm walls of seeds as storage polysaccharides (Meier and Reid, 1982). In the cell wall, structural polysaccharides that may interact with cellulose, both Glc and Man are found in the mannan backbone (Moreira and Filho, 2008), and these polysaccharides are consequently known as glucomannans. Glucomannans are highly abundant in the cell walls of early land plants, such as mosses and lycophytes (Moller et al., 2007; Scheller and Ulvskov, 2010). Mannan and glucomannan backbone Man residues may be substituted at O-6 with a single α-Gal or at O-2/O-3 with acetyl groups. The presence of substitutions on the mannan backbone determines its properties and varies between different species and tissues (Timell, 1965; Northcote, 1972). Galactosylated glucomannan is known as galactoglucomannan (GGM). GGM has high industrial importance, as it is the most abundant noncellulosic polysaccharide in gymnosperm (softwood) secondary cell walls, constituting up to 20% of the plant dry mass (Willför et al., 2008). GGM has also been found in various angiosperm plant primary cell walls, such as tobacco (*Nicotiana plumbaginifolia*) cell cultures (Sims et al., 1997), kiwifruit (*Actinidia deliciosa*; Schröder et al., 2001), and tomato (*Solanum lycopersicum*) fruit (Tong and Gross, 1988; Seymour et al., 1990).

The role of GGM in cell walls is unclear. It may have a signaling role in plant development (Goubet et al., 2003; Benová-Kákosová et al., 2006; Liepman et al., 2007; Iglesias-Fernández et al., 2011). Like other hemicelluloses, it may also coat and crosslink cellulose fibrils (Fry, 1986; Iiyama et al., 1994; Obel et al., 2007). The molecular basis of GGM binding to cellulose microfibrils is unknown and may involve hydrogen bonding and stacking interactions (Berglund et al., 2016). It has been hypothesized that the conformation of glucomannan chains in the cell wall is similar to those of cellulose, showing a relatively flat 2-fold screw axis, with Gal substitutions also able to interact with the cellulose surfaces (Aspinall et al., 1962; Northcote, 1972; Whitney et al., 1998; Moreira and Filho, 2008). Consistent with the proposed role in binding to cellulose, studies incorporating structurally distinct mannans into synthetic composites have shown that glucomannan from konjac (*Amorphophallus konjac*) and salep (*Orchis mascula*) induces coalescence of cellulose fibrils and reduction of cellulose crystallinity (Hackney et al., 1994; Whitney et al., 1998). Moreover, the extent of association of legume seed galactomannan with cellulose fibrils was positively correlated with decreased Gal content of the galactomannan (Whitney et al., 1998). In angiosperms, the dominance of GGM is reduced compared to gymnosperms, and xylan is the main secondary cell wall hemicellulose, yet GGM is always present. Xylan has recently been shown to interact with the hydrophilic surface and perhaps also the hydrophobic surface of cellulose microfibrils as a 2-fold helical screw (Busse-Wicher et al., 2014; Simmons et al., 2016; Grantham et al., 2017). Due to the reported random heterogeneous nature of the GGM backbone and the presence of acetate and Gal substitutions, it is unclear if GGM can interact with the cellulose microfibril in a xylan-like fashion.

The glucomannan backbone, synthesized by the Cellulose Synthase-Like A (CSLA) family of enzymes, is thought to have a random Man and Glc sequence (Northcote, 1972; Piro et al., 1993; Liepman et al., 2005). In vitro, CSLA enzymes use either or both GDP-Man and GDP-Glc to synthesize pure mannan/glucan or glucomannan backbones (Dhugga et al., 2004; Liepman et al., 2005). Mannan Synthesis-Related proteins may also be involved in glucomannan synthesis (Wang et al., 2013). Arabidopsis (*Arabidopsis thaliana*) Trichome Birefringence-Like25 and 26 have been hypothesized to be involved in the *O*-acetylation of glucomannan, but no experimental evidence has yet been provided (Gille et al., 2011). The frequency and distribution of the Gal side chains on galactomannan is in part a feature of the galactosyltransferase enzyme specificity (Reid et al., 2003). In vitro activity of fenugreek (*Trigonella foenumgraecum*) GalactoMannan GalactosylTransferase (*Tf*GMGT) demonstrated that this enzyme can transfer α-Gal from UDP-Gal to β-1,4-linked mannan oligosaccharides (Edwards et al., 1999, 2002). On the basis of sequence similarity to *Tf*GMGT, two enzymes in Arabidopsis, which we now name MANNANα-GALACTOSYLTRANSFERASE1(MAGT1/GlycosylTransferase-Like6/MUCILAGE-RELATED10 [MUCI10], At2g22900) and MAGT2 (GlycosylTransferase 6, At4g37690), are thought to be involved in the α-1,6-Gal substitution in Arabidopsis GGM (Faik et al., 2002; Dunkley et al., 2006; Vuttipongchaikij et al., 2012; Voiniciuc et al., 2015), but the activity has not yet been conclusively demonstrated and the acceptor specificity has not been studied.

In Arabidopsis, when mature dry seeds are hydrated, gel-like mucilage is extruded to envelop the entire seed. Ruthenium red staining of Arabidopsis seeds reveals two different mucilage layers, termed the nonadherent and the adherent mucilage layers (Western et al., 2000). Arabidopsis seed mucilage is an excellent model system for understanding cell wall structure and biosynthesis (Haughn and Western, 2012). CSLA2 and MAGT1/MUCI10 have been demonstrated to participate in the synthesis of GGM present in mucilage (Yu et al., 2014; Voiniciuc et al., 2015). Mutation of either *CSLA2* or *MAGT1* caused smaller and more compact mucilage capsules, decreased cellulose crystallinity, and changed pectin distribution. This suggests that mucilage GGM, synthesized by CSLA2 and MAGT1, may interact with cellulose and other cell wall components (Voiniciuc et al., 2015). The absence of CSLA2 resulted in a significant loss of Gal, Glc, and Man residues in mucilage, almost in a 1:1:1 molar ratio (Yu et al., 2014). Consistent with its proposed role in GGM

[1]This work was supported by the Leverhulme Trust Centre for Natural Material Innovation (L.Y. and P.D.), by studentship from the Biotechnology and Biological Sciences Research Council (BBSRC) of the UK as part of the Cambridge BBSRCDTP Program (reference BB/J014540/1) for J.J.L., the Open Plant Synthetic Biology Research Centre (J.J.L. and P.D., reference BB/L014130/1), FAPESP Grant 2013/08293-7 (C.S.P. and M.S.S.), the Ministry of Education, Culture, Sports, Science, and Technology of Japan (Grant-in-Aid for Scientific Research no. 24114006 to T.K.), and by a studentship from The Low Carbon Energy University Alliance (A.L.).

[2]Current address: Aspire BioScience, 12635 E. Montview Blvd., Aurora, Colorado 80045.

[3]Author for contact: pd101@cam.ac.uk.

[4]Senior author.

The author responsible for distribution of materials integral to the findings presented in this article in accordance with the policy described in the Instructions for Authors (www.plantphysiol.org) is: Paul Dupree (pd101@cam.ac.uk).

L.Y. conceived the project, designed the experiments, performed experiments, analyzed the data, and wrote the article with contributions of all the authors; J.J.L. performed the construct preparation and contributed to the enzyme expression and article writing; C.S.P. designed, performed, and analyzed MD simulations; T.K. contributed to the early stages of design of the project; X.Y. performed the isolation of homozygous T-DNA insertion mutants; A.L. provided technical assistance to L.Y. for MS experiments; S.M. initiated studies on MAGT1 activity; M.S.S. supervised and analyzed MD experiments and contributed to the writing; P.D. conceived the project, designed and supervised the experiments, analyzed the data, and wrote the article.

[OPEN]Articles can be viewed without a subscription.

www.plantphysiol.org/cgi/doi/10.1104/pp.18.00709

galactosylation, the *magt1/muci10* mutant also showed the reduction of Gal, Glc, and Man residues but with significantly greater reductions of Gal compared with Glc and Man (Voiniciuc et al., 2015).

Here, we demonstrate that Arabidopsis seed mucilage GGM has a defined patterned structure, having a backbone consisting of a two-residue repeating unit: [4)-β-Glc-(1,4)-β-Man-(1,]. Most Man residues are substituted with single α-Gal residues. CSLA2 is responsible for the biosynthesis of the mucilage glucomannan backbone, and MAGT1 catalyses the addition of α-Gal to mannosyl residues. In vitro activity assays demonstrated that MAGT1 is highly specific, transferring α-Gal from UDP-Gal to Man of glucomannan oligosaccharides only when the acceptor has sufficient Glc-Man disaccharide repeating units. Molecular dynamics simulations suggest that this patterned glucomannan is able to interact with certain cellulose fibril faces as a 2-fold screw, providing a potential explanation for the structure of this polysaccharide and suggesting modes of interaction of this hemicellulose with cellulose.

RESULTS

Arabidopsis Mucilage Glucomannan Has a Repeating Disaccharide [4)-β-Glc-(1,4)-β-Man-(1,] Backbone

The mannan content of Arabidopsis seed mucilage is less than 5% (w/w) of total sugars, and the structure is unclear. Based on monosaccharide compositional and linkage analysis and studies of GGM structure in other plants, Voiniciuc et al. (2015) suggested that the mucilage GGM has a Man:Glc ratio of 3:1, and one in every two Man residues is substituted by a single α-1,6-Gal, and one in every six Man might be substituted with a β-1,2-Gal-α-1,6-Gal disaccharide. To investigate the fine structure of GGM in seed mucilage, we employed enzymatic digestion with β-mannanase 26A (Man26A; Handford et al., 2003; Gilbert, 2010). Man26A displays specificity for Man at the −1 subsite, but can tolerate Glc at the +1 subsite and hence can cleave β-Man-(1,4)-β-Glc, but not β-Glc-(1,4)-β-Man. Substitution of Man at the −1 subsite by Gal or acetate is not tolerated (Malgas et al., 2015; von Freiesleben et al., 2016). Alcohol insoluble residue (AIR) from seed mucilage was incubated with alkali to solubilize and deacetylate the hemicelluloses before digestion with Man 26A. The released oligosaccharides were labeled with the fluorophore 8-amino-naphthalene-1,3,6-trisulfonic acid (ANTS) and separated by electrophoresis (polysaccharide analysis using carbohydrate gel electrophoresis [PACE]; Goubet et al., 2002). This procedure yielded a notably simple ladder of oligosaccharides from adherent mucilage of wild-type Arabidopsis (Fig. 1A; Supplemental Fig. S1). The migration differences suggested the oligosaccharides might differ in degree of polymerization (DP) by at least two hexose residues, with the smallest oligosaccharide migrating slightly slower than mannotetraose (M_4). Two oligosaccharides with relatively high abundance were visible, but larger oligosaccharides were detected with a lower abundance. Similar oligosaccharides were observed after nonadherent mucilage digestion (Supplemental Fig. S2). In contrast to the wild type, adherent mucilage from *csla2* yielded no detectable oligosaccharides (Fig. 1A), indicating that CSLA2 is necessary for the GGM backbone synthesis in seed mucilage, which is consistent with previous publications (Yu et al., 2014; Voiniciuc et al., 2015). To look for any undigested GGM, we first digested wild-type adherent mucilage with β-mannanase Man26A and then used 65% ethanol to precipitate any resistant GGM from the released oligosaccharides. The monosaccharide compositions of the Man26A-resistant residue from wild-type mucilage and of *csla2* mutant mucilage (lacking the relevant GGM) were compared. This analysis revealed no significant difference in sugar composition between the two samples (Supplemental Table S1). Thus, we can conclude that Man26A is likely digesting all CSLA2-synthesized GGM into oligosaccharides.

In order to characterize the backbone structure of the adherent mucilage GGM further, Man26A products from wild type were digested with α-galactosidase. All the released oligosaccharides were sensitive to the galactosidase (Fig. 1B), indicating the widespread presence of α-Gal decorations on the backbone. After the removal of Gal side chains, the glucomannan oligosaccharides, named saccharide S1 to S6, were subjected to cycles of alternating β-glucosidase and β-mannosidase treatments (Fig. 1B). For example, after incubation with β-glucosidase, the enzyme was deactivated and then β-mannosidase was added. This approach enabled us to deduce their Man and Glc sequence. The high-intensity band S2, migrating between M_5 and M_6, shows the procedure for structural analysis of all oligosaccharides S1 through to S6. After the first cycle of β-glucosidase digestion, S2 changed its migration to a position between M_4 and M_5, indicating the presence of Glc on the nonreducing end of S2. This first cycle β-glucosidase product of S2 was then treated with β-mannosidase, and the released oligosaccharide migrated to the position between M_3 and M_4. A second cycle of β-glucosidase shifted the migration to a position between M_2 and M_3. A second cycle of β-mannosidase digestion released the disaccharide β-Glc-(1,4)-Man (GM). In summary, the sequence of Man and Glc in S2 is Glc-Man-Glc-Man-Glc-Man. All other oligosaccharides showed the same sensitivities to alternate β-glucosidase and β-mannosidase digestion, suggesting that they might all be composed of the repeating disaccharide [4)-β-Glc-(1,4)-β-Man-(1,].

To confirm the size of the Man26A oligosaccharide products and the linkage of the backbone residues, they were digested with α-galactosidase, labeled with 2-aminobenzamide (2-AB) and then analyzed by matrix-assisted laser-desorption ionization time of flight (MALDI-TOF) mass spectrometry (MS) and tandem mass spectrometry (MS/MS). The MS revealed

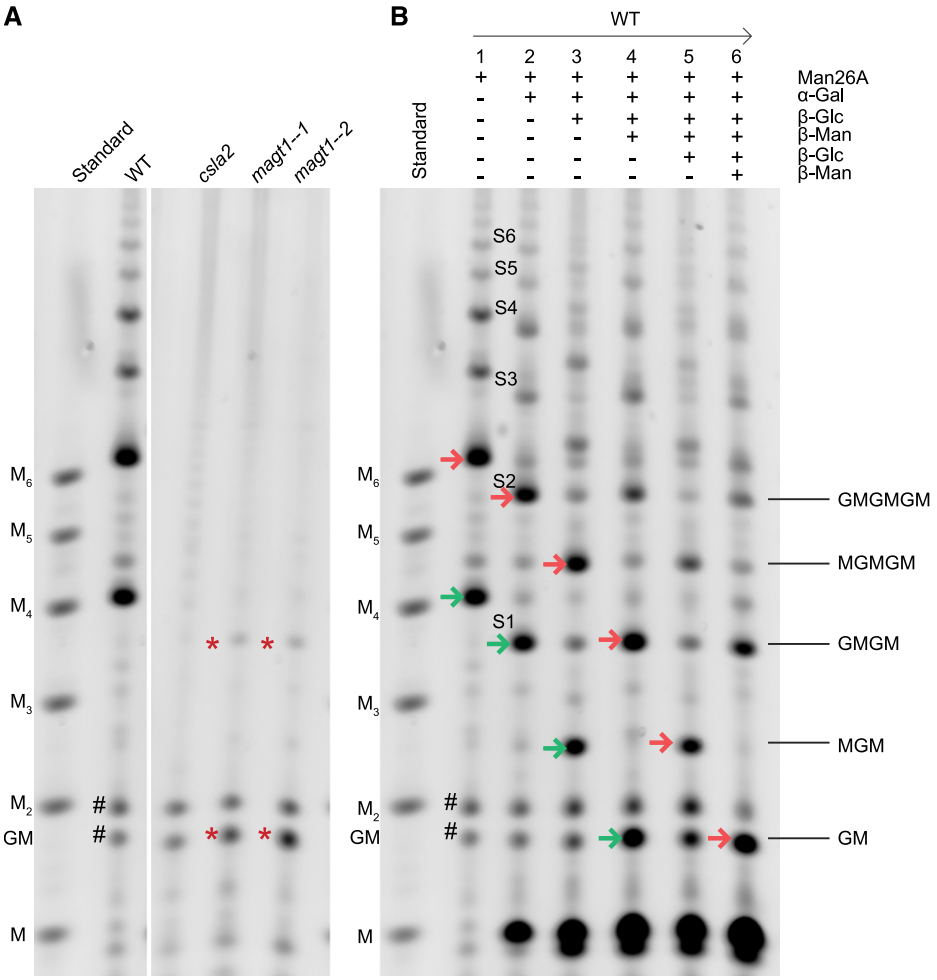

Figure 1. Mannan backbone structure in adherent mucilage. A, PACE gel of mannanase (Man26A)-digested deacetylated hemicellulose from adherent mucilage of wild type (WT), *csla2*, and two *magt1* mutant lines. B, Characterization of Man26A-digested products by PACE, using *α*-galactosidase (*α*-Gal), *β*-glucosidase (*β*-Glc), and/or *β*-mannosidase (*β*-Man) enzymes. Mannan oligosaccharides, M_1–M_6. On the right of B, interpreted oligosaccharides structures with G, Glc, and M, Man. Arrows with the same color follow the oligosaccharides through sequential digestion. Asterisks show mannan oligosaccharides in adherent mucilage from two *magt1* mutant lines after Man26A digestion. Hash shows the background bands.

two main peaks with mass corresponding to hexose$_4$ ((Hex)$_4$; *m/z* 809.3, [M+Na]$^+$) and (Hex)$_6$ (*m/z* 1133.4, [M+Na]$^+$), corresponding to oligosaccharides S1 and S2, respectively (Fig. 2A). MS/MS indicated that S1 is a linear oligosaccharide of four hexoses (indicated by Y_{1-3} and $^{1,5}X_{1-3}$ ion series) linked by 1,4 linkages (indicated by $^{3,5}A_{2-3}$ and G_{1-3} ions; Fig. 2B). S2 is a linear oligosaccharide of six hexoses (indicated by Y_{1-5} and $^{1,5}X_{1-5}$ ion series) linked by 1,4-linkages (indicated by $^{3,5}A_{2-5}$ and G_{1-5} ions; Fig. 2C). Taken together, the enzyme sensitivities revealed by PACE and the MS fragmentation show that S1 has a structure of [4)-*β*-Glc-(1,4)-*β*-Man-(1,]$_2$ and that S2 has a structure of [4)-*β*-Glc-(1,4)-*β*-Man-(1,]$_3$. Given their similar enzyme sensitivities and the product mobilities, we can deduce that the other oligosaccharides, S3 to S6, also have a backbone with the [4)-*β*-Glc-(1,4)-*β*-Man-(1,]$_n$ structure.

The Majority of the Glc-Man Backbone Disaccharide Units Have an *α*-Gal Decoration on the Man Residue

To determine the position of the *α*-Gal side chains on the backbone of mucilage GGM, Man26A digestion products without *α*-galactosidase digestion were labeled with 2-AB and analyzed with MS. The MS spectra revealed two main peaks of mass corresponding to (Hex)$_5$ (*m/z* 971.3 [M+Na]$^+$) and (Hex)$_8$ (*m/z* 1457.3 [M+Na]$^+$; Fig. 3A), suggesting S1 is substituted by a single Gal and S2 by two Gal residues. MS/MS of (Hex)$_5$ revealed a branched oligosaccharide (Fig. 3B). The 324 D mass difference between Y_2 and Y_3 ions suggests that the first Man from the nonreducing end is modified with the Gal. The presence of the V_3 elimination ions (*m/z* 599.2) and $^{3,5}A_2$ cross ring fragment (*m/z* 583.1) indicate that a single Gal is linked at the *O*6 of the first Man residue from the nonreducing end of the S1 backbone.

MS/MS spectra of (Hex)$_8$ (*m/z* 1457.3) confirmed the S2 oligosaccharide (Fig. 3C), [4)-*β*-Glc-(1,4)-*β*-Man-(1,]$_3$, as the backbone with *α*-1,6-linked Gal on the first and second Man from the nonreducing end. These results are consistent with the reported positions of *α*-Gal decorations solely on Man residues of GGM (Aspinall et al., 1962; Northcote, 1972). Taken together with the *α*-galactosidase sensitivity of the hexose branches, this MS analysis indicates the presence of a single *α*-Gal substitution on each Man except the reducing-end Man of the oligosaccharide. The absence of Gal

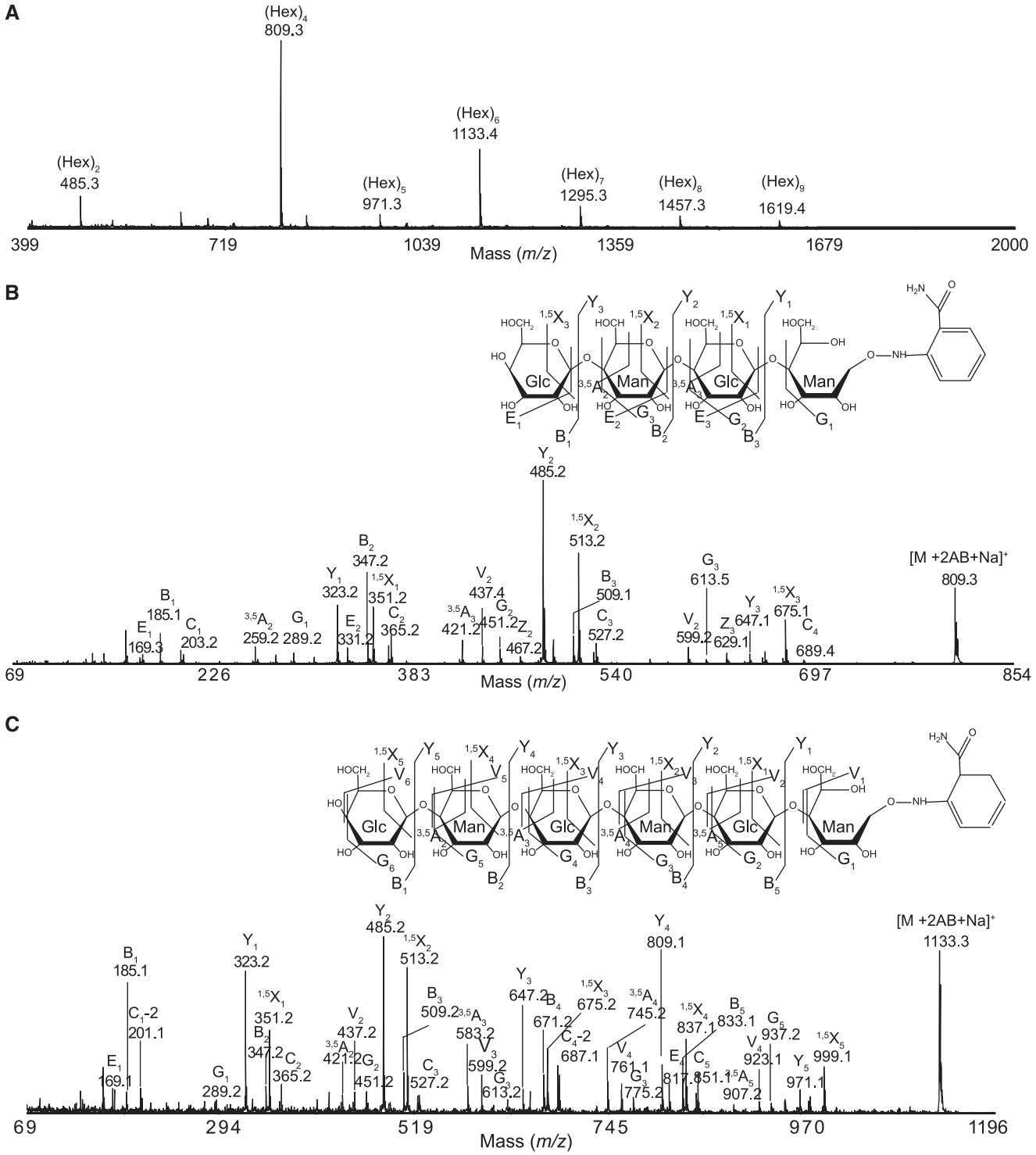

Figure 2. Man26A- and then α-galactosidase-digested products of wild-type adherent mucilage AIR were confirmed as linear. A, Man26A- and then α-galactosidase-digested products of adherent mucilage AIR were labeled with 2-AB and analyzed by MALDI-TOF MS. B and C, $(Hex)_4$ and $(Hex)_6$ in A were identified to be linear by MS/MS. Glc and Man assignments are based on the PACE results.

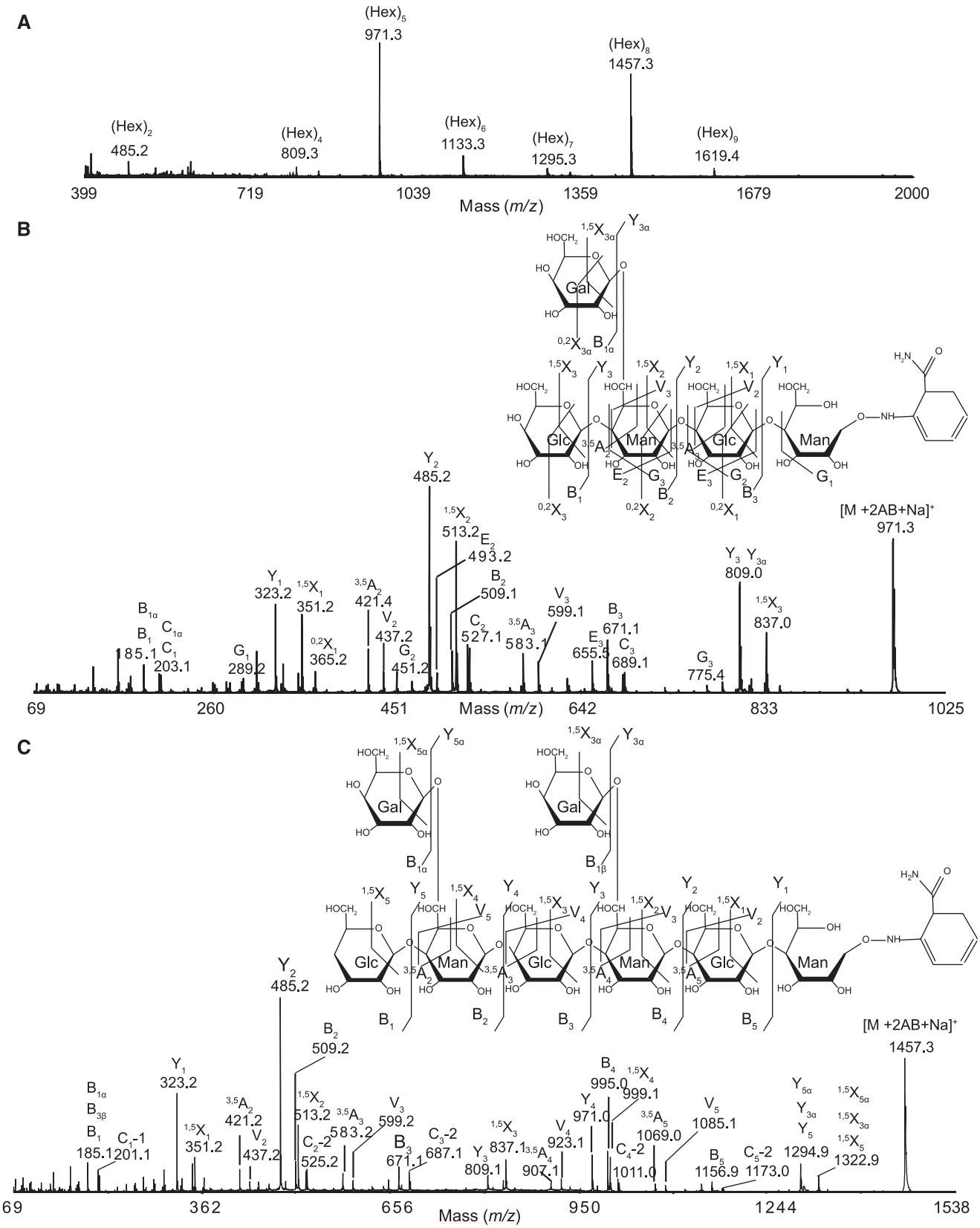

Figure 3. All mannosyl residues on the glucomannan backbone except that on the reducing end were substituted by single α-Gal at C-6. A, Man26A-digested products of adherent mucilage AIR were labeled with 2-AB and analyzed by MALDI-TOF-MS. B and C, $(Hex)_5$ and $(Hex)_8$ in A were analyzed by high-energy MALDI-CID.

substitution of the reducing-end Man residue is consistent with known requirements of mannanases.

To evaluate the ratio of Man:Glc:Gal in the GGM, Man26A products of wild-type adherent mucilage were extracted with 65% ethanol, and the monosaccharide composition was analyzed. The results showed that the ratio of Man:Glc:Gal in the Man26A products of wild-type adherent mucilage digestion was approximately 3:3:2.2 (Supplemental Table S1).

No Acetyl Groups Were Detected on Seed Mucilage GGM

To determine if the GGM in seed mucilage is acetylated, adherent mucilage AIR was digested with Man26A without further pretreatment, labeled with 2-anthranilic acid (2-AA) and then analyzed by MS. The MS spectra show two main peaks of mass corresponding to $(Hex)_5$ (*m/z* 972.3) and $(Hex)_8$ (*m/z* 1458.3; Supplemental Fig. S3), without evidence of acetylation and similar to the alkaline extracted GGM. This result demonstrated that seed mucilage GGM is not acetylated.

MAGT1 Is Responsible for the Addition of α-Gal to the Glucomannan Backbone in Seed Mucilage

MAGT1/MUCI10/GlycosylTransferase-Like6 from Arabidopsis is a Golgi-localized putative glycosyltransferase in CAZy family GT34 (Coutinho et al., 2003), and a homolog of the *Tf*GMGT from fenugreek endosperm, suggesting it might be a GGM α-galactosyltransferase (Faik et al., 2002; Dunkley et al., 2006; Voiniciuc et al., 2015). In addition, the Gal content was significantly decreased in seed mucilage of the *magt1/muci10* mutant (Voiniciuc et al., 2015). To determine whether MAGT1 is responsible for α-Gal substitutions to the CSLA2 glucomannan, we analyzed the GGM in two *magt1* T-DNA insertion lines by PACE. Man26A digestion of *magt1-1* mucilage AIR released low-abundance oligosaccharides that comigrated with S1 and β-Glc-(1,4)-Man (Fig. 1A). Further digestion with alternate β-glucosidase and β-mannosidase confirmed *magt1-1* oligosaccharides were identical to S1 and β-Glc-(1,4)-Man (Fig. 4). Interestingly, these two oligosaccharides were much less abundant than the oligosaccharides released from wild type, confirming that digestible glucomannan content is decreased in *magt1* mucilage.

In Vitro MAGT1 Is Active Only on Glucomannan Acceptor Composed of the Repeating Glc-Man Disaccharide

To investigate the biochemical activity of MAGT1, we transiently expressed a MAGT1-Myc fusion protein by infiltration of *Nicotiana benthamiana* leaves with *Agrobacterium tumefaciens* carrying the appropriate construct. We also expressed a *Picea glauca* Xylan GlucUronylTransferase (*Pg*GUX) enzyme (Lyczakowski et al., 2017) as a control to ensure that the activity observed was not associated with expression of a Golgi-localized glycosyltransferase. Immunoblot analysis confirmed

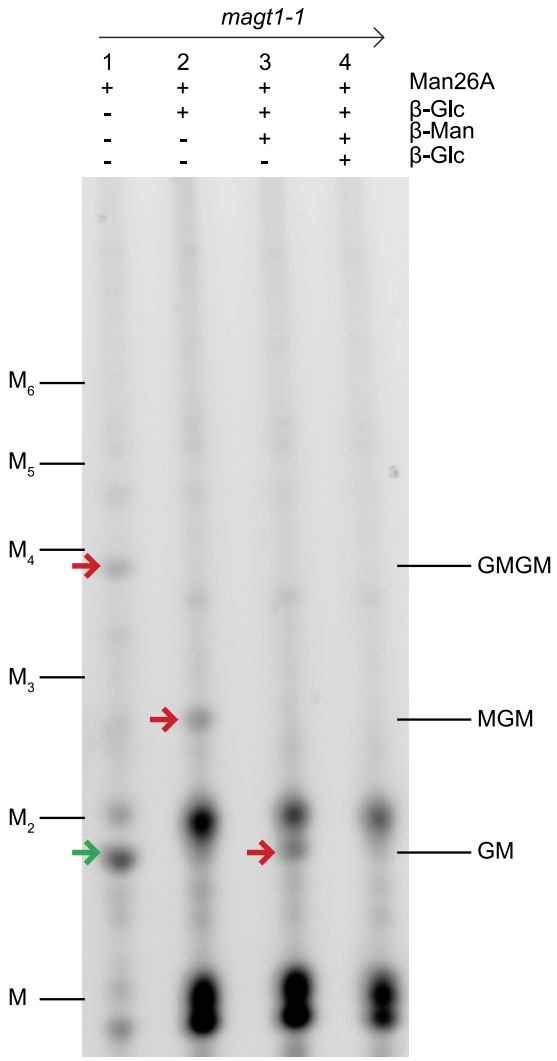

Figure 4. *magt1-1* glucomannan structure analyzed by PACE. *magt1-1* adherent mucilage AIR was digested with Man26A and then digested with β-glucosidase (β-Glc) and β-mannosidase (β-Man) alternatively. All the products were then labeled with ANTS and analyzed with PACE. Mannan oligosaccharides, M_1–M_6; G, Glc; M, Man. Arrows with the same color show the band flow direction after sequential digestion.

that microsomes isolated from *N. benthamiana* leaves contained Myc-tagged proteins with sizes corresponding to monomers and dimers of MAGT1 and monomers of spruce *Pg*GUX (Supplemental Fig. S4). Microsomes extracted from the infiltrated plants were used directly for the galactosyltransferase activity assays.

MAGT1 acts on the $(Glc\text{-}Man)_n$-patterned glucomannan backbone in mucilage biosynthesis. Therefore, to act as an appropriate acceptor for the in vitro activity assays, a mixture mainly of $(Glc\text{-}Man)_2$ (S1) and $(Glc\text{-}Man)_3$ (S2) oligosaccharides lacking Gal was prepared by mannanase and galactosidase sequential digestion of wild-type adherent mucilage (Fig. 5A). The acceptor was labeled with the ANTS fluorophore for visualization. After 5 h reaction with microsomes and UDP-Gal,

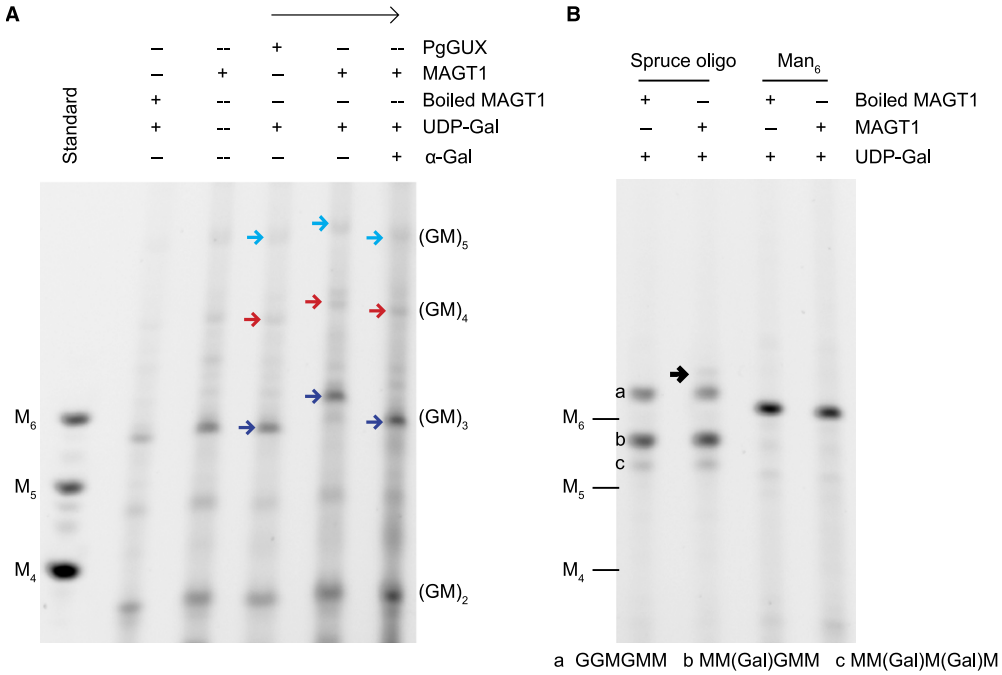

Figure 5. Activity of recombinant MAGT1 protein. A, MAGT1 activities using Glc-Man repeating oligosaccharides as the acceptor. B, MAGT1 activities using spruce oligosaccharides and Man_6 as the acceptors. Arrows with the same color show the band flow direction after each reaction. Black arrow shows the very weak product of MAGT1. Mannan oligosaccharides, M_4–M_6; G, Glc; M, Man.

the products were analyzed by PACE (Fig. 5A). In the reaction containing MAGT1, UDP-Gal as a donor and $(Glc\text{-}Man)_n$ oligosaccharides as an acceptor, the $(Glc\text{-}Man)_3$ DP6 oligosaccharide disappeared, and a new band with slower migration appeared, putatively due to Gal substitution of this oligosaccharide. This shift in mobility was not seen in the absence of UDP-Gal or when microsomes containing PgGUX were used. Digestion of the MAGT1 products with α-galactosidase caused the oligosaccharides to migrate as before the reaction, confirming that MAGT1 has α-galactosyltransferase activity onto glucomannan. The activity was seen only with acceptors with a DP6 backbone or longer.

To determine whether MAGT1 can use a range of mannan and glucomannan acceptors, several other acceptors in a mixture of GGM oligosaccharides from spruce wood (see preparation procedure in Supplemental Fig. S5), and Man_6 were tested. The spruce wood galactoglucomannan oligo sample contained three oligosaccharides: Glc-Glc-Man-Glc-Man-Man (structure "a"), Man-(Gal)Man-Glc-Man-Man (structure "b"), and Man-(Gal)Man-(Gal)Man-Man (structure "c"). With MAGT1 microsomes and UDP-Gal, the intensity of these three oligosaccharides from spruce wood did not substantially change, indicating they are less favorable substrates compared to the mucilage glucomannan oligosaccharides (Fig. 5B). One very weak oligosaccharide, migrating slightly slower than structure "a," appeared in the reaction products. This suggested that MAGT1 had very weak activity with one or more of these three oligosaccharides. Oligosaccharide "a" contains a Glc-Man-Glc-Man tetrasaccharide within its structure and was likely the poor acceptor. MAGT1 also could not use mannohexaose as the acceptor (Fig. 5B) as described before (Voiniciuc et al., 2015). These results indicate that MAGT1 shows activity specific to the patterned (Glc-Man) backbone synthesized by CSLA2. The effective oligosaccharides were DP6 or longer.

Molecular Dynamics Simulations Suggest Modes of GGM Binding to Cellulose

The precise patterning of the GGM from Arabidopsis seed mucilage, with a two-residue periodic repeat, suggested the structure might have an ability to align and interact with cellulose fibrils. We performed molecular dynamics (MD) simulations to investigate the interaction between the patterned GGM and cellulose. We built a patterned GGM model in which the backbone consisted of the repeating disaccharide Glc-Man, where Glc and Man appeared in every odd and even position, respectively. The DP of the GGM model chain was 24 with a backbone of 16 residues and eight side-chain Gal residues. All Man residues were α-1,6 linked to Gal (Fig. 6A). We considered 36-chain and 18-chain crystalline cellulose fibrils (Ding and Himmel, 2006; Thomas et al., 2013), both of them with DP 24 glucan chains (Fig. 6, B and C). GGM chains were initially placed on the 36-chain fibril in parallel with cellulose chains on the hydrophilic (1-10), (110), and hydrophobic (200) faces and also in antiparallel alignment on the (110), (1-10), and (100) faces (Fig. 6B). For the 18-chain cellulose fibril, glucomannan chains were aligned parallel to cellulose on hydrophilic (010) and hydrophobic (200) faces and antiparallel on (020) and (100) surfaces (Fig. 6C).

To study the stability of the interaction, we performed three independent simulations of each system

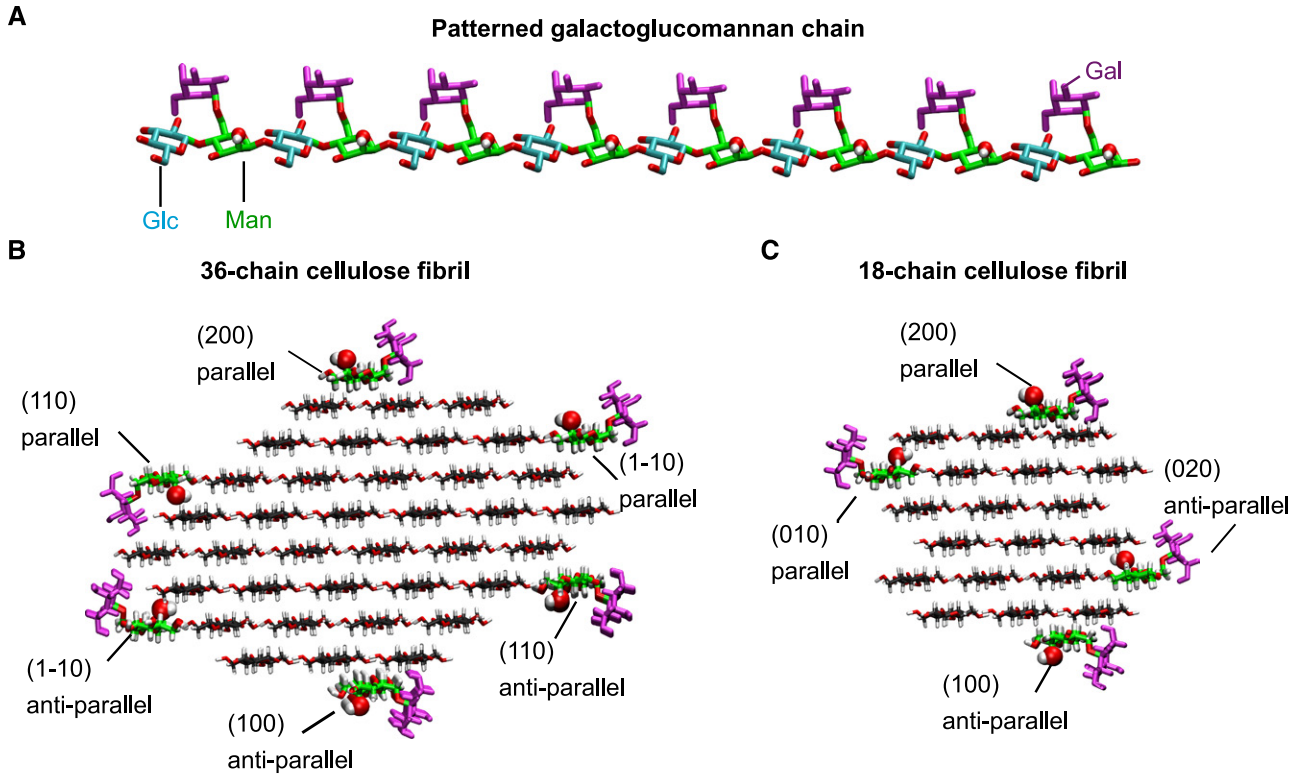

Figure 6. Molecular models built to perform molecular dynamics simulations. A Arabidopsis seed mucilage patterned galactoglucomannan model. B and C, Complexes of galactoglucomannan and cellulose fibrils. The axial C-2 hydroxyls from Man residues are highlighted by van der Waals spheres. The reducing ends of the parallel galactoglucomannan chains are at the reducing ends of the glucan chains of the cellulose microfibril, while the reducing ends of the antiparallel galactoglucomannan chains are at the nonreducing ends of the glucan chains of the cellulose fibril.

and left out of the subsequent analysis the two first and last residues. Figure 7, C–L, shows the time evolution of the root mean squared deviation (rmsd) for each GGM chain relative to its initial position at the start of each run. The patterned GGM remained stably bound to all cellulose faces, with rmsd values less than 3 Å, except for the parallel configuration on face (110) and antiparallel on (1-10), as shown in Figure 7, G and H. Randomly picked snapshots are depicted in Figure 7, A and B, for visualization. Because Man differs from Glc by an axial, instead of equatorial, hydroxyl group at C-2 position, the GGM chains in parallel to cellulose on face (110) and antiparallel on face (1-10) experienced unfavorable steric contacts with cellulose via the axial hydroxyl groups from Man (Fig. 6B), which, in turn, rendered GGM chains more mobile on these particular cellulose surfaces. Similar steric effects were also present on faces (010) and (020) of the 18-chain cellulose fibril, but in this case, stabilizing GGM-cellulose interactions due to the existence of grooves in the fibril prevented dissociation of GGM from the cellulose surface (Fig. 7, I–L).

Figure 8 shows the two-dimensional distribution of GGM backbone configurations, defined by the minimum distance of glucomannan residues from the cellulose surface and by the sum of glycosidic torsion angles $\varphi + \psi$. Minimum distances lower than 3 Å indicate that the chain is tightly bound to cellulose. The result shows that only the chain placed in parallel on the (110) face visited configurations with distances greater than 3 Å (Fig. 8E). The sum $\varphi + \psi$ indicates the degree of helicity, where $\varphi + \psi = 120°$, $\varphi + \psi = 190°$, and $\varphi + \psi = 50°$ characterize 2-fold (2_1), left-handed 3-fold (3_1), and right-handed 3_1 screw conformations, respectively. The chains adsorbed in parallel on faces (200) adopt mostly 2_1 screw conformation, with $\varphi + \psi = 120°$ (Fig. 8, A and G). The $\varphi + \psi$ distributions for chains adsorbed in antiparallel on face (100), parallel on face (1-10), antiparallel on face (110), parallel on face (010), and antiparallel on face (020) exhibit two local maxima at approximately 90° and 150° (Fig. 8, B–D, I, and J), with an average $\varphi + \psi$ value of 120°, indicating 2_1 screw-like conformation, as previously observed for xylan adsorption on cellulose (Busse-Wicher et al., 2016). The decrease of intramolecular hydrogen bonds increases chain flexibility relative to cellulose chains. In patterned GGM chains, the Man axial hydroxyl groups (O-2) are not in position to hydrogen bond to the O-6 from neighboring Glc, and α-1,6-Gal branches restrict the O-6 conformations and decrease the hydrogen bond frequency between Man residues and O-3 from Glc (Fig. 8K). Therefore, the glucomannan backbone adopts a 2_1 screw-like

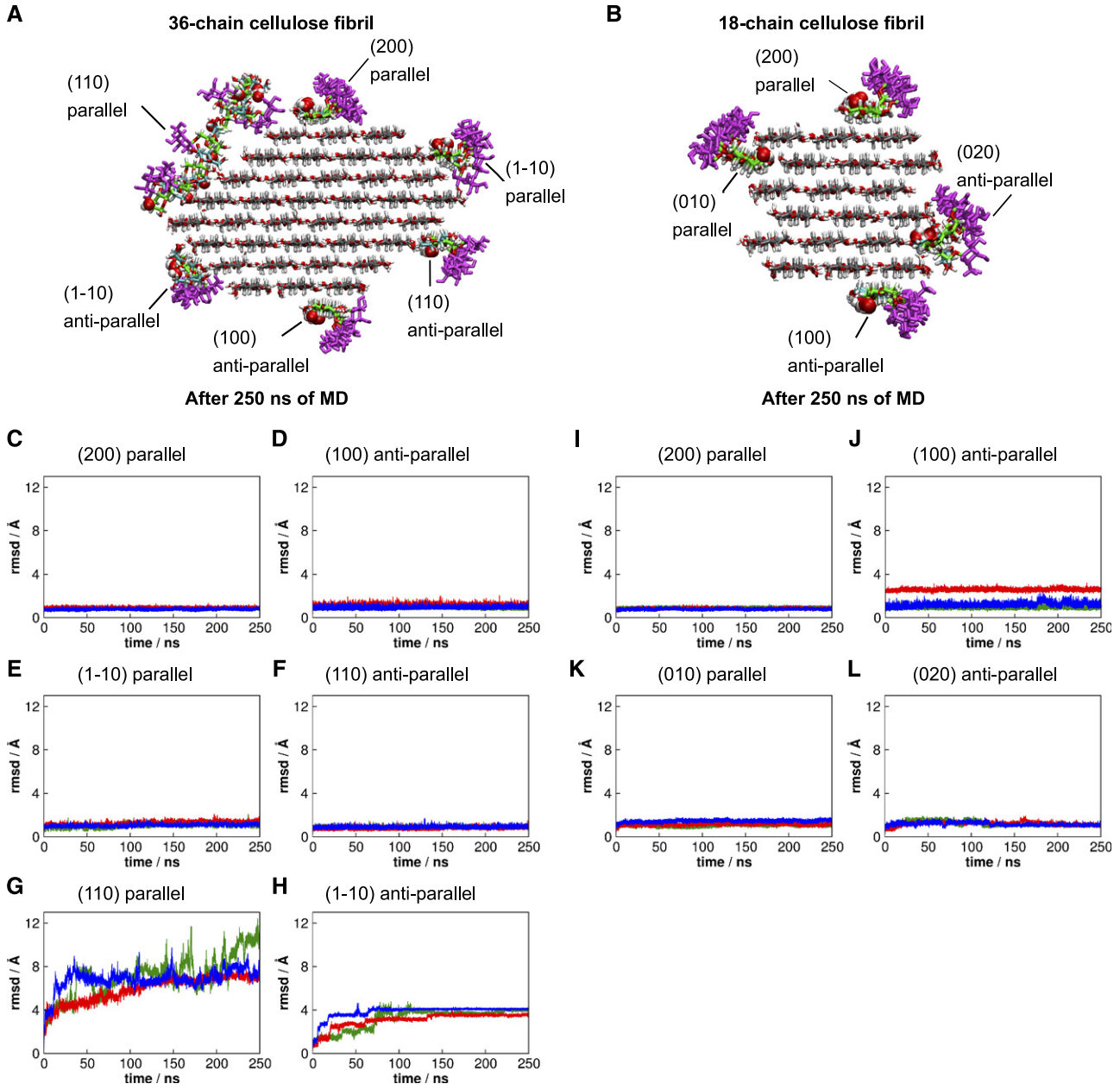

Figure 7. Binding analysis of patterned galactoglucomannan on cellulose surfaces. A and B, Snapshots illustrating the systems after 250 ns of molecular dynamics simulation. C to H, Root mean squared deviation (rmsd) of galactoglucomannan chains from its initial position on 36-chain cellulose surfaces. I to L, Rmsd of galactoglucomannan chains from its initial position on 18-chain cellulose surfaces. The different colors represent different independent simulations.

conformation instead of the ideal 2_1 screw conformation. Similarly, the antiparallel chain on the (100) surface is displaced from the ideal 2_1 screw to accommodate the Gal branches (Fig. 8H).

DISCUSSION

Aside from the steric role of α-galactosyl side chains, any importance of the GGM fine structure for interactions with other polymers in plant cell walls is poorly understood. Here, we show that the Arabidopsis seed mucilage GGM backbone has a strictly alternating structure of a glucosyl residue and a mannosyl residue. Moreover, we demonstrate that a little more than two in three of the mannosyl residues are substituted with an α-galactosyl branch. CSLA2 and MAGT1 are required for the biosynthesis of this GGM. This precisely repetitive structure may enable GGM synthesized by CSLA2 and MAGT1 to bind hydrophobic surfaces of cellulose fibrils and also perhaps some hydrophilic surfaces.

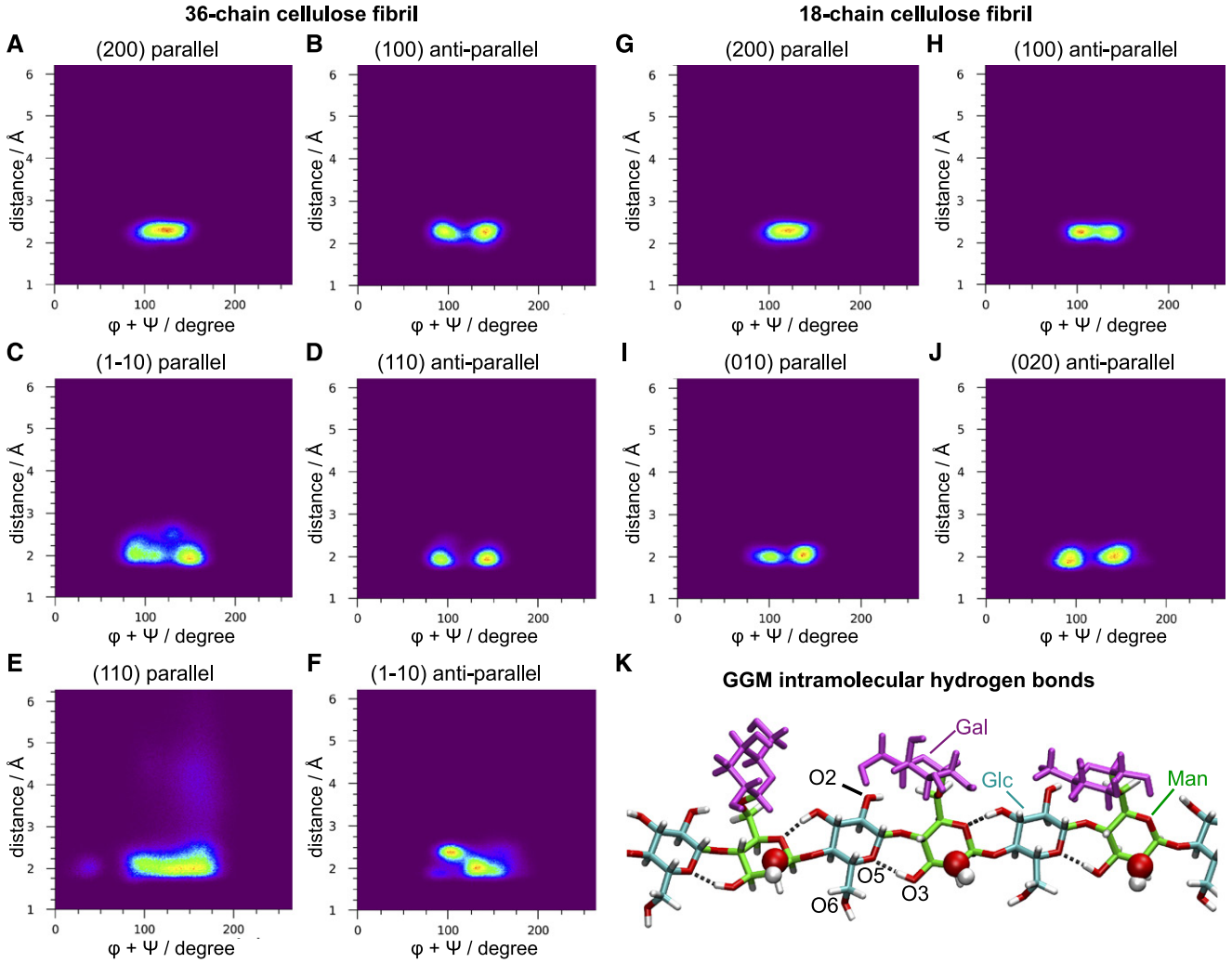

Figure 8. Patterned galactoglucomanann backbone conformations on cellulose surfaces. A to F, Two-dimensional distribution of the minimum distance of galactoglucomanann residues from 36-chain cellulose surface and sum of glycosidic torsion angles $\varphi + \psi$. G to J, Two-dimensional distribution of the minimum distance of galactoglucomanann residues from 18-chain cellulose surface and sum of glycosidic torsion angles $\varphi + \psi$. K, Snapshot illustrating the intramolecular hydrogen bonds from galactoglucomannan. The axial hydroxyl from Man residues are highlighted by van der Waals spheres.

GGM is generally thought to have a random arrangement of Glc and Man and occasional Gal substitution and acetylation on the mannosyl residues (Piro et al., 1993; Scheller and Ulvskov, 2010; Voiniciuc et al., 2015). Here, we studied GGM oligosaccharides using specific enzymatic digestion and gel electrophoresis (PACE) and were able to separate oligosaccharides with identical mass, but different composition or order of Glc and Man residues (Goubet et al., 2002; Handford et al., 2003). We found that Arabidopsis seed mucilage GGM has a backbone consisting of a repeating disaccharide [4)-β-Glc-(1,4)-β-Man-(1,]. We did not detect acetylation of this patterned GGM. Many of the Man residues in the backbone are substituted by single α-1,6-Gal, yielding a polymer with the ratio of Glc:Man:Gal of approximately 3:3:2.2. Since alternate backbone residues are Man carrying a Gal substitution, these Gal substitutions are evenly spaced along the backbone. GGMs with similar backbone structures have been isolated from tobacco (*Nicotiana plumbaginifolia*) cell cultures and kiwifruits, but these GGMs show less α-Gal substitution of the Man and also have β-Gal-(1,2)-α-Gal- side chains (Sims et al., 1997; Schröder et al., 2001). It will be interesting to determine how widespread this strictly patterned GGM is in plant tissues.

CSLA2 and MAGT1 Synthesize Patterned GGM

We observed that CSLA2 is exclusively responsible for the patterned GGM backbone synthesis in Arabidopsis seed mucilage, leading to the complete loss of detectable GGM in *csla2* mucilage. It has been reported by monosaccharide composition analysis that *csla2* mucilage still has some Man remaining (Yu et al., 2014;

Voiniciuc et al., 2015), but it is possible that Man detected in these studies is derived from glycans attached to glycosylated proteins in mucilage or Man26A does not have access to a remaining population of mucilage mannan. The finding that CSLA2 produces GGM with a repeating disaccharide [4)-β-Glc-(1,4)-β-Man-(1,] backbone is consistent with earlier monosaccharide composition analysis, which demonstrated that Man and Glc decreased by the same amount in *csla2* mucilage compared to wild-type mucilage (Yu et al., 2014; Voiniciuc et al., 2015). Earlier studies on glucomannan structure in Arabidopsis stems, which is synthesized mostly by CSLA9, suggested the arrangement of Glc and Man is random in the backbone (Handford et al., 2003; Goubet et al., 2009). It appears therefore that CSLA2 has an unexpected precision in glucomannan biosynthesis in mucilage-producing cells. It is conceivable that the GT2 CSLA2 enzyme is able to incorporate the sugars alternately from GDP-Glc and GDP-Man into the growing polysaccharide chain, even though it is likely to have a single active site (Stone et al., 2010). This implies that the presence of terminal Man on the acceptor could favor binding of GDP-Glc to the donor site in the enzyme, and likewise terminal Glc might favor binding of GDP-Man. The production of a polysaccharide backbone with alternating sugars by other GT2 β-glycan polysaccharide synthases has been previously reported. For example, the prokaryotic hyaluronan synthases incorporate both GlcA and GlcNAc alternately (DeAngelis and Weigel, 1994). In plants, both CSLF and CSLH enzymes are able to make β-Glc-(1,4)- and β-Glc-(1,3)- linkages in the backbone, with a nonrandom distribution (Stone et al., 2010), further suggesting the acceptor can influence the catalytic site activity of GT2 enzymes. On the other hand, Liepman et al. (2005) demonstrated that the recombinant CSLA2 expressed in insect cells can use GDP-Man and/or GDP-Glc to synthesize homomannan or glucomannan, but the enzyme had higher activity when GDP-Man was supplied. Perhaps, in mucilage-producing cells the supply of sugar nucleotides or interaction with other Golgi proteins might influence the CSLA2 activity to enable a strict alternation in substrates.

We showed that MAGT1 is a specific glucomannan galactosyltransferase required for the addition of α-Gal on the patterned CSLA2 glucomannan backbone. Previous work showed that MAGT1/MUCI10 likely decorates the glucomannan synthesized by CSLA2 in Arabidopsis seed mucilage (Voiniciuc et al., 2015). We confirm here that the mucilage glucomannan from *magt1* mutants completely lacks the Gal substitution, and the glucomannan backbone can be digested into disaccharide β-Glc-(1,4)-β-Man, and tetrasaccharide β-Glc-(1,4)-β-Man-(1,4)-β-Glc-(1,4)-β-Man. Previous attempts to carry out in vitro galactosyltransferase activity assays of this Arabidopsis GT34 enzyme have had little success (Vuttipongchaikij et al., 2012; Voiniciuc et al., 2015). Our in vitro assay showed that MAGT1 has effective galactosyltransferase activity, but only when the patterned CSLA2 glucomannan is supplied as the acceptor. MAGT1 appears to require at least three (Glc-Man) disaccharide repeating units for maximal galactosylation activity in vitro. No or little activity toward other tested glucomannan acceptors, such as Man_6, was detected, confirming that MAGT1 selectively galactosylates GGM backbones. The strong preference of MAGT1 for the correct patterned acceptor may explain why previous attempts to assay this galactosyltransferase activity have been unsuccessful.

In *magt1* mutants, the amount of CSLA2 synthesized GGM backbone was strongly reduced. Gal substitution is likely to improve the solubility of GGM (Timell, 1965; Northcote, 1972). In *magt1*, without the addition of α-Gal, newly synthesized glucomannan polysaccharides may precipitate, affecting the further elongation of the backbone. In addition, *magt1* seed mucilage is very sticky, so the poorly soluble glucomannan lacking α-Gal may be lost during the sample preparation. An alternative hypothesis is that CSLA2 and MAGT1 form a protein complex. Therefore, the absence of MAGT1 may affect the CSLA2 protein stability, targeting, or function, as has been suggested for CSLC in the absence of xyloglucan xylosyltransferase enzymes (Cocuron et al., 2007).

Patterned GGM May Interact with Cellulose Fibrils with a 2-Fold Screw Conformation

What could be the function of such a precisely patterned GGM made by CSLA2 and MAGT1? It is now well established that the even periodic spacing of glucuronosyl, arabinosyl, and acetate residues on xylan facilitates its alignment along and stable interaction with hydrophilic surfaces of cellulose fibers as a 2-fold helical screw (Busse-Wicher et al., 2014, 2016; Simmons et al., 2016; Grantham et al., 2017). The disaccharide repeating unit in this GGM is suggestive of a role in the alignment with cellulose, because like cellulose-bound xylan, this GGM has an even periodic repeat. Here, we showed using MD simulations that the GGM chains can effectively bind to different faces of two distinct models of cellulose fibrils by adopting 2-fold helical screw or 2-fold screw-like conformations. The binding can occur on certain hydrophilic faces and also on the hydrophobic faces, as seen with xylan (Busse-Wicher et al., 2014; Martínez-Abad et al., 2017). In the case of xylan, the even substitution pattern allows binding to cellulose by avoiding steric clashes on hydrophilic faces. Our modeling suggests that the even spacing of Man residues in the patterned GGM provides a particular advantage for binding to hydrophobic cellulose faces because steric hindrance between cellulose and both the mannosyl C-2 hydroxyl groups and the α-Gal substitutions is avoided.

Previous studies of structurally distinct storage glucomannans and galactomannans incorporated into mannan-cellulose synthetic composites suggested that the structural differences in Glc and Man are not critical for mannan binding to cellulose (Hackney et al., 1994; Whitney et al., 1998). However, it was not possible

to distinguish with which microfibril surfaces these storage mannans interacted. Our simulation results showed that the patterned GGM structure may have a particular advantage for binding the hydrophobic face of the cellulose microfibril. This binding is facilitated by a lack of steric hindrance between the mannosyl residues of glucomannan and Glc of cellulose because all the mannosyl C-2 hydroxyl groups face away from the fibril (Fig. 7). However, this C-2 hydroxyl group inhibits the binding of glucomannan to certain hydrophilic faces of the fibril (Fig. 7, G and H). This modeling therefore indicates that mannosyl C-2 hydroxyl groups could be important for modulating the GGM and cellulose interaction.

Association of seed storage galactomannan with cellulose fibrils, agarose, and xanthan was reported to be positively correlated with decreasing Gal substitution (Dea et al., 1986; Hackney et al., 1994; Whitney et al., 1998). The Gal substitutions sterically inhibited self-association of the galactomannan and the binding to cellulose. The GGM described in this study is different to the galactomannan used for these in vitro mannan-cellulose interaction assays, because the arrangement of the Gal substitutions in mucilage GGM is not random (Dea et al., 1986; Hackney et al., 1994; Whitney et al., 1998). The modeling suggests the Gal substitution of the patterned GGM may have less of a steric influence on binding to cellulose. When bound to cellulose fibrils in the 2-fold screw conformation, all the Gal side chains of the patterned GGM project away from the cellulose surface. The Gal side chains of the GGM bound to cellulose may play a role in preventing aggregation of cellulose in the "cellulose rays" of mucilage, because the lack of GGM causes the cellulose fibrils to aggregate in *csla2* or *magt1* mucilage.

It will be important to determine if similar cellulose-compatible, patterned, GGM structures exist in cell types beyond Arabidopsis mucilage, such as in softwoods from conifers where acetylated GGM is the main hemicellulose that interacts with the cellulose.

MATERIALS AND METHODS

Reagents

All chemicals were purchased from Sigma-Aldrich unless otherwise described.

Plant Material and Growth Conditions

All Arabidopsis (*Arabidopsis thaliana*) plants were of Col-0 ecotype. T-DNA insertion line *csla2* (SALK_065083) has been described previously (Goubet et al., 2009). T-DNA insertion lines *magt1-1* (SALK_061576) and *magt1-2* (SALK_002556) were selected from the Nottingham Arabidopsis Stock Centre. All the primers used are shown on Supplemental Table S2. Arabidopsis seeds were surface sterilized, sown on Murashige and Skoog medium, stratified in darkness for 48 h at 4°C and then germinated at 21°C under 16-h light/8-h dark conditions. After 1 to 2 weeks, the seedlings were transferred to soil and grown in growth chambers under the same conditions.

Nicotiana benthamiana plants were grown in the same conditions as Arabidopsis. Leaves of 4-week old *N. benthamiana* were used for infiltration.

Seed Mucilage Extraction

Two grams of clean seeds were incubated in 20 mL of deionized water with gentle shaking for 2 h at room temperature. The resulting suspension was centrifuged at 1,000 rpm for 1 min. The supernatant was collected, and the seeds were washed twice with deionized water. Three batches of supernatants were pooled and freeze-dried to get nonadherent mucilage. After water extraction, seeds were taken to the ball-mill tube and 20 mL of deionized water was added. The seed-containing tubes were shaken for 30 min at 30 Hz in a Retsch MM400 ball mill using two adaptors. The seed suspension was centrifuged at 1,000 rpm for 1 min. The supernatant was collected and the seeds were washed twice with deionized water. Three batches of supernatant were collected and freeze-dried to get adherent mucilage.

Preparation of Mucilage Hemicelluloses

Freeze-dried mucilage was washed twice with 65% ethanol (v/v), twice with 80% ethanol (v/v), and twice with 100% ethanol (v/v). The pellet was then air-dried to obtain mucilage AIR. To release mannan for digestion, 80 mg of mucilage AIR was treated with 2.5 mL of 4 M NaOH at room temperature for 1 h and centrifuged at 4,000 rpm for 15 min. In order to neutralize the NaOH, prior to enzymatic digestion, the supernatants were loaded onto a PD-10 desalting column (GE Life Science) and eluted with 50 mM ammonium acetate (pH 6.0) according to the manufacturer's instructions. The eluent contained the majority of the deacetylated hemicelluloses and was aliquoted into 10 tubes for 10 reactions.

Enzyme Digestion of Mannans

The eluted hemicelluloses fraction was digested with an excess of *Cellvibrio japonicus* Man26A in 50 mM ammonium acetate (pH 6.0) at 37°C overnight and then deactivated. Man26A products were then digested overnight with *Cellvibrio mixtus* GH27 α-galactosidase in 50 mM sodium acetate (pH 6.0) at 37°C to remove the α-Gal side chains. For sequential digestion, enzymes used were *Aspergillus niger* GH3 β-glucosidase and *C. mixtus* GH5 β-mannosidase. The digestion conditions were 50 mM ammonium acetate (pH 6.0) at 37°C for 3 h with excess enzymes to complete digestion. After each reaction, samples were boiled at 100°C for 10 min to denature the enzyme. Samples were then dried at 60°C in vacuo.

Adherent mucilage can also be digested directly with Man26A in 50 mM ammonium acetate (pH 6.0) at 37°C overnight and then heat deactivated. The sample was then dried at 60°C in vacuo. One mL of 65% ethanol was added to the dry sample, which was then centrifuged at 10,000 rpm for 10 min. The supernatants were then dried at 60°C in vacuo and analyzed by MALDI-TOF MS.

Preparation of Samples for Monosaccharide Composition Analysis

The eluted hemicelluloses fraction was digested with Man26A as above and then heat deactivated. The sample was then dried at 60°C in vacuo. One mL of 65% ethanol was added to the dry sample, which was then centrifuged at 10,000 rpm for 30 min. The supernatants and pellets were then dried at 60°C in vacuo and hydrolyzed with 2 M trifluoroacetic acid (TFA).

TFA Hydrolysis and Monosaccharide Composition Analysis

Adherent mucilage after different treatments was hydrolyzed with 2 M TFA at 121°C for 1 h. Following TFA evaporation under vacuum, the samples were resuspended in 200 mL of water, and the monosaccharide sugars were separated using protocols adapted from Currie and Perry (2006) on a Dionex ICS3000 system equipped with a PA20 column, a PA20 guard column, and a borate trap (Dionex; Tryfona et al., 2012).

Mannan Fingerprint Analysis by PACE

Samples and M_{1-6} standards (Megazyme) were derivatized with ANTS (Invitrogen) as described previously (Goubet et al., 2002). After drying, the samples were resuspended in 100 µL of 3 M urea, of which 2 µL was loaded onto the PACE gels. The samples were run and visualized using a G-box equipped

with a transilluminator with long-wavelength light tubes (365 nm) and a short pass filter (500–600 nm) as described previously (Goubet et al., 2002). All analyses of GGM were repeated a minimum of three times.

Preparation of Oligosaccharides for MS

Following the enzyme digestion, released peptides and enzymes were removed using reverse-phase Sep-Pak C18 cartridges (waters) as previously described. The GGM oligos were reductively aminated with 2-AB or 2-AA, using optimized labeling conditions as previously described. The labeled samples were then purified from reductive amination regents using a GlycoClean S cartridge (Prozyme) as described previously (Tryfona et al., 2010).

Hydrophilic Interaction Liquid Chromatography (HILIC)

Capillary HILIC was carried out using an LC-Packings Ultimate system (Dionex), which was used to generate the gradient that flowed at 3 mL min^{-1}. Solvent A was 50 mM ammonium formate adjusted to pH 4.4 with formic acid. Solvent B was 5% solvent A in acetonitrile. The labeled oligosaccharides dissolved in 95% acetonitrile were loaded onto an amide-80 column (300 mm × 325 cm, 3 mm particle size; Dionex) and eluted with increasing aqueous concentrations as described previously (Tryfona et al., 2012). The following gradient conditions were applied: 0 min, 5% solvent A, 95% solvent B; 6 min, 25% solvent A, 75% solvent B; 86 min, 45% solvent A, 55% solvent B. The column eluent passed through a capillary UV detector (set at 254 nm) to the MALDI sample spotter. For HILIC-MALDI-TOF/TOF-MS/MS, a Probot sample fraction system (Dionex) was employed for automated spotting of the HPLC eluent onto a MALDI target at 20-s intervals. After air drying, the sample spots were overlaid with 2,5-dihydroxybenzoic acid matrix and analyzed by MALDI-TOF/TOF-MS/MS as described above (Tryfona et al., 2012).

Preparation and Structural Determination of Spruce Oligosaccharides for in Vitro Assay

AIR from Norway spruce (*Picea abies*) sawdust was prepared as described previously (Bromley et al., 2013). Spruce AIR was treated with 4 M NaOH for 1 h, neutralized with 2 M acetic acid, dialyzed against distilled water, and then freeze-dried to get deacetylated hemicellulose.

Deacetylated hemicellulose was dissolved in 50 mM ammonium acetate and digested with excess Man26A at 37°C overnight. Man26A products were then separated by size-exclusion chromatography on a gravity-driven Bio-Gel P2 column (2.5 × 90 cm; Bio-Rad) and eluted with 50 mM ammonium acetate. Fractions (2 mL) were collected and analyzed by PACE as described as above. Fraction A with mannan oligosaccharides migrated around M_6 was combined.

For the unsubstituted glucomannan in fraction A, sequential digestion with β-glucosidase and β-mannosidase was performed as above. For the Gal-substituted oligosaccharides, fraction A was treated with a combination of β-glucosidase and β-mannosidase first to remove unsubstituted glucomannan, then with α-galactosidase to remove Gal side chains, and finally sequentially digested with β-glucosidase and β-mannosidase to determine the backbone.

Preparation of Acceptors for the in Vitro α-Galactosyltransferase Assay

Three types of oligosaccharides were used as the substrate for the MAGT1 assay. $(Glc\text{-}Man)_n$ oligosaccharides were prepared by digestion of WT adherent mucilage hemicelluloses with Man26A and then α-galactosidase. A mixture of galactoglucomannan oligosaccharides (fraction A) was purified from spruce wood. The third oligosaccharide is mannohexaose (Megazyme). Oligosaccharides for reactions were derivatized with ANTS as described above. Nonderivatized fluorophores were removed using a GlycoClean S cartridge as described above and the labeled acceptors were dried at 30°C in vacuo.

Preparation of Overexpression Vectors and *N. benthamiana* Infiltration

3×Myc-tagged *MAGT1* (At2g22900) and Spruce *PgGUX* coding sequences were PCR amplified from previously described constructs (Lyczakowski et al., 2017) using primers described in Supplemental Table S2. The coding sequence (CDS) was blunt end ligated into a *Nru*I-digested pEAQ-HT vector (Sainsbury et al., 2009). The construct was transformed into competent AGL-1 *Agrobacterium tumefaciens* using a freeze-thaw method. On the day of infiltration, 5 mL of an overnight AGL-1 culture was used to inoculate 20 mL of Lysogeny broth supplemented with ampicillin (100 µg/mL) and kanamycin (50 µg/mL). Following 8 h of incubation at 30°C, 200 rpm, the culture reached OD_{600} 0.6 and was ready for infiltration into *N. benthamiana* leaves. The infiltration of leaves with AGL-1 was performed as previously described (Sparkes et al., 2006).

Microsome Preparation and Immunoblot Analysis

Entire infiltrated leaves were harvested on day 3 after infiltration. All microsome preparation steps took place at 4°C. *N. benthamiana* leaf tissue was ground in homogenization buffer (50 mM HEPES-KOH, pH 6.8, 0.4 M Suc, 1% PVPP, 1 µM PMSF, and 1 complete protease inhibitor tablet [Roche]/50 mL buffer), strained through a nitrocellulose mesh and centrifuged at 3,000 rpm for 10 min to remove cellular debris. The supernatant was centrifuged at 15,000 rpm for 1 h at 4°C. The resulting pellets were combined and concentrated at 15,000 rpm for 30 min. Microsomes were used immediately or frozen in liquid nitrogen and stored at −80°C.

Microsomal protein concentration was quantified using a modified Bradford assay according to the manufacture's instruction (Expedeon). For immunoblot analysis, 5 µg protein were resolved by SDS-PAGE on 4% to 15% gradient gels (Bio-Rad) and blotted onto nitrocellulose membranes (GE Healthcare) using iBlot system (GE Life Sciences). Blots were probed with 1:1,000 dilution of mouse anti-Myc antibody (Santa-Cruz Biotech, A14), followed with a 1:10,000 dilution of goat anti-mouse antibody conjugated to horseradish peroxidize (Bio-Rad, 170-6515). Blots were visualized using an Amersham ECL Prime western Blotting Detection Reagent and Amersham Hyperfilm (GE Life Sciences).

α-Galactosyltransferase Assay

The 30-µL reaction mixture consisting of UDP-Gal (5 mM; Promega), DTT (0.25 mM), $MnCl_2$ (5 mM), $MgCl_2$ (5 mM), and Triton X-100 (1% v/v) was added to a tube containing dried acceptor. For negative controls, the reactions were stopped by heating at 100°C for 10 min. The reaction mixture was amended with 30 µL of microsome. Samples were incubated at room temperature for 5 h with shaking. The reaction was stopped by heating at 100°C for 10 min. To remove lipids, the sample was subjected to the chloroform-methanol phase separation method as previously described (Bligh and Dyer, 1959). The aqueous phase was collected and dried at 30°C in vacuo. To further confirm if the acceptor was substituted by α-Gal, products were digested with excess of α-galactosidase in 50 mM ammonium acetate (pH 6.0) at 37°C for 6 h and then the reaction was stopped by heating at 100°C for 10 min and dried at 30°C in vacuo. All the products were resuspended in 20 µL of 3 M urea and separated using the PACE method as described above. All transferase assays were repeated at least twice.

Molecular Dynamics Simulations

The cellulose models of 36-chain and 18-chain elementary fibrils were obtained by Cellulose-Builder (Gomes and Skaf, 2012), considering the Iβ polymorph (Nishiyama et al., 2002) and degree of polymerization of 24. Glucan chains with degree of polymerization 24 were placed in parallel with cellulose chains on (1-10), (200), and (110), in antiparallel on (110), (100), and (1-10) faces on 36-chain cellulose fibril, in parallel on faces (010) and (200), and in antiparallel on (020) and (100) faces from 18-chain cellulose fibril. To obtain patterned galactoglucomannan chains, the equatorial hydroxyl groups from the even residues were removed and axial hydroxyl groups added to generate Man units. Subsequently, α-1,6 Gal branches were added to all Man residues. The axial hydroxyl groups and Gal branches were added using CHARMM36 force-field internal coordinates (Guvench et al., 2009; Raman et al., 2010). The systems of 36-chain and 18-chain fibril in complex with glucomannan chains were immersed in a box of water, such that the solvent layer was 16 Å thick around the cellulose-glucomannan complex.

Simulations were performed using NAMD (Phillips et al., 2005), with the CHARMM36 force field for carbohydrates (Guvench et al., 2009; Raman et al., 2010) and the TIP3P water model (Jorgensen et al., 1983). Simulations were carried out under periodic boundary conditions. Electrostatic interactions were treated via particle mesh Ewald (Darden et al., 1993), and short-range interactions were cutoff at 12 Å. The temperature was kept at 300 K with Langevin

thermostat, and pressure was controlled at 1 bar with a Langevin piston (Phillips et al., 2005). A time step of 2 fs was used to solve the equations of motion. Chemical bonds involving hydrogen atoms were constrained at their equilibrium lengths.

The systems were submitted to the following steps: (1) 100 steps of energy minimization and 500 ps of MD with only the solvent and Gal atoms free to move; (2) same as (1), but with cellulose atoms C-1, C-2, C-3, C-4, C-5, and O-5 harmonically restrained to prevent distortions, with a force constant of 50 kcal mol^{-1} $Å^{-2}$. (3) 250 ns of MD were generated in triplicate for each system with only cellulose atoms restrained, as in (2). Subsequent analyses were performed over these trajectories using in-house codes and VMD (Humphrey et al., 1996).

Accession Numbers

Sequence data for the genes employed in this study are as follows: *MAGT1*, At2g22900; *CSLA2*, At5g22740.

Supplemental Data

The following supplemental materials are available.

Supplemental Figure S1. PACE gel of control samples of undigested material and enzymes.

Supplemental Figure S2. Mannan backbone structure in nonadherent mucilage.

Supplemental Figure S3. No evidence for the acetylation of the mannan oligosaccharides.

Supplemental Figure S4. Immunoblot of Myc-tagged recombinant proteins expressed in *N. benthamiana*.

Supplemental Figure S5. Preparation and structural determination of spruce oligos for in vitro assays.

Supplemental Table S1. Monosacchairdes composition of adherent mucilage after different treatments.

Supplemental Table S2. Primers used in this study.

ACKNOWLEDGMENTS

The authors would like to acknowledge Prof. George Lomonossoff (John Innes Centre, UK), who developed the pEAQ-HyperTrans expression system used in this study. Plant Bioscience Limited supplied the pEAQ-HT vector that was used in this work.

Received July 31, 2018; accepted August 21, 2018; published September 5, 2018.

LITERATURE CITED

Aspinall GO, Begbie R, McKay JE (1962) 40. The hemicelluloses of European larch (*Larix decidua*). Part II. The glucomannan component. J Chem Soc **0**: 214–219

Benová-Kákosová A, Digonnet C, Goubet F, Ranocha P, Jauneau A, Pesquet E, Barbier O, Zhang Z, Capek P, Dupree P, (2006) Galactoglucomannans increase cell population density and alter the protoxylem/metaxylem tracheary element ratio in xylogenic cultures of Zinnia. Plant Physiol **142**: 696–709

Berglund J, Angles d'Ortoli T, Vilaplana F, Widmalm G, Bergenstråhle-Wohlert M, Lawoko M, Henriksson G, Lindström M, Wohlert J (2016) A molecular dynamics study of the effect of glycosidic linkage type in the hemicellulose backbone on the molecular chain flexibility. Plant J **88**: 56–70

Bligh EG, Dyer WJ (1959) A rapid method of total lipid extraction and purification. Can J Biochem Physiol **37**: 911–917

Bromley JR, Busse-Wicher M, Tryfona T, Mortimer JC, Zhang Z, Brown DM, Dupree P (2013) GUX1 and GUX2 glucuronyltransferases decorate distinct domains of glucuronoxylan with different substitution patterns. Plant J **74**: 423–434

Busse-Wicher M, Gomes TC, Tryfona T, Nikolovski N, Stott K, Grantham NJ, Bolam DN, Skaf MS, Dupree P (2014) The pattern of xylan acetylation suggests xylan may interact with cellulose microfibrils as a twofold helical screw in the secondary plant cell wall of Arabidopsis thaliana. Plant J **79**: 492–506

Busse-Wicher M, Li A, Silveira RL, Pereira CS, Tryfona T, Gomes TC, Skaf MS, Dupree P (2016) Evolution of xylan substitution patterns in gymnosperms and angiosperms: implications for xylan interaction with cellulose. Plant Physiol **171**: 2418–2431

Cocuron JC, Lerouxel O, Drakakaki G, Alonso AP, Liepman AH, Keegstra K, Raikhel N, Wilkerson CG (2007) A gene from the cellulose synthase-like C family encodes a beta-1,4 glucan synthase. Proc Natl Acad Sci USA **104**: 8550–8555

Coutinho PM, Deleury E, Davies GJ, Henrissat B (2003) An evolving hierarchical family classification for glycosyltransferases. J Mol Biol **328**: 307–317

Currie HA, Perry CC (2006) Resolution of complex monosaccharide mixtures from plant cell wall isolates by high pH anion exchange chromatography. J Chromatogr A **1128**: 90–96

Darden T, York D, Pedersen L (1993) Particle mesh Ewald: An $N{\cdot}\mathrm{Log}(N)$ method for Ewald sums in large systems. J Chem Phys **98**: 10089–10092

Dea ICM, Clark AH, McCleary BV (1986) Effect of galactose-substitution-patterns on the interaction properties of galactomannans. Carbohydr Res **147**: 275–294

DeAngelis PL, Weigel PH (1994) Immunochemical confirmation of the primary structure of streptococcal hyaluronan synthase and synthesis of high molecular weight product by the recombinant enzyme. Biochemistry **33**: 9033–9039

Dhugga KS, Barreiro R, Whitten B, Stecca K, Hazebroek J, Randhawa GS, Dolan M, Kinney AJ, Tomes D, Nichols S, (2004) Guar seed β-mannan synthase is a member of the cellulose synthase super gene family. Science **303**: 363–366

Ding SY, Himmel ME (2006) The maize primary cell wall microfibril: a new model derived from direct visualization. J Agric Food Chem **54**: 597–606

Dunkley TP, Hester S, Shadforth IP, Runions J, Weimar T, Hanton SL, Griffin JL, Bessant C, Brandizzi F, Hawes C, (2006) Mapping the Arabidopsis organelle proteome. Proc Natl Acad Sci USA **103**: 6518–6523

Edwards ME, Dickson CA, Chengappa S, Sidebottom C, Gidley MJ, Reid JS (1999) Molecular characterisation of a membrane-bound galactosyltransferase of plant cell wall matrix polysaccharide biosynthesis. Plant J **19**: 691–697

Edwards ME, Marshall E, Gidley MJ, Reid JS (2002) Transfer specificity of detergent-solubilized fenugreek galactomannan galactosyltransferase. Plant Physiol **129**: 1391–1397

Faik A, Price NJ, Raikhel NV, Keegstra K (2002) An Arabidopsis gene encoding an α-xylosyltransferase involved in xyloglucan biosynthesis. Proc Natl Acad Sci USA **99**: 7797–7802

Fry SC (1986) Cross-linking of matrix polymers in the growing cell walls of angiosperms. Ann Rev Plant Physiol37: 165–186

Gilbert HJ (2010) The biochemistry and structural biology of plant cell wall deconstruction. Plant Physiol **153**: 444–455

Gille S, de Souza A, Xiong G, Benz M, Cheng K, Schultink A, Reca IB, Pauly M (2011) O-acetylation of Arabidopsis hemicellulose xyloglucan requires AXY4 or AXY4L, proteins with a TBL and DUF231 domain. Plant Cell **23**: 4041–4053

Gomes TCF, Skaf MS (2012) Cellulose-builder: a toolkit for building crystalline structures of cellulose. J Comput Chem **33**: 1338–1346

Goubet F, Jackson P, Deery MJ, Dupree P (2002) Polysaccharide analysis using carbohydrate gel electrophoresis: a method to study plant cell wall polysaccharides and polysaccharide hydrolases. Anal Biochem **300**: 53–68

Goubet F, Misrahi A, Park SK, Zhang Z, Twell D, Dupree P (2003) AtCSLA7, a cellulose synthase-like putative glycosyltransferase, is important for pollen tube growth and embryogenesis in Arabidopsis. Plant Physiol **131**: 547–557

Goubet F, Barton CJ, Mortimer JC, Yu X, Zhang Z, Miles GP, Richens J, Liepman AH, Seffen K, Dupree P (2009) Cell wall glucomannan in Arabidopsis is synthesised by CSLA glycosyltransferases, and influences the progression of embryogenesis. Plant J **60**: 527–538

Grantham NJ, Wurman-Rodrich J, Terrett OM, Lyczakowski JJ, Stott K, Iuga D, Simmons TJ, Durand-Tardif M, Brown SP, Dupree R, (2017) An even pattern of xylan substitution is critical for interaction with cellulose in plant cell walls. Nat Plants **3**: 859–865

Guvench O, Hatcher ER, Venable RM, Pastor RW, Mackerell AD (2009) CHARMM additive all-atom force field for glycosidic linkages between hexopyranoses. J Chem Theory Comput **5**: 2353–2370

Hackney JM, Atalla RH, VanderHart DL (1994) Modification of crystallinity and crystalline structure of Acetobacter xylinum cellulose in the presence of water-soluble β-1,4-linked polysaccharides: 13C-NMR evidence. Int J Biol Macromol **16**: 215–218

Handford MG, Baldwin TC, Goubet F, Prime TA, Miles J, Yu X, Dupree P (2003) Localisation and characterisation of cell wall mannan polysaccharides in Arabidopsis thaliana. Planta **218**: 27–36

Haughn GW, Western TL (2012) Arabidopsis seed coat mucilage is a specialized cell wall that can be used as a model for genetic analysis of plant cell wall structure and function. Front Plant Sci **3**: 64

Humphrey W, Dalke A, Schulten K (1996) VMD: visual molecular dynamics. J Mol Graph **14**: 33–38, 27–28

Iglesias-Fernández R, Rodríguez-Gacio MC, Barrero-Sicilia C, Carbonero P, Matilla A (2011) Three endo-β-mannanase genes expressed in the micropylar endosperm and in the radicle influence germination of *Arabidopsis thaliana* seeds. Planta **233**: 25–36

Iiyama K, Lam T, Stone BA (1994) Covalent cross-links in the cell wall. Plant Physiol **104**: 315–320

Jorgensen WL, Chandrasekhar J, Madura JD, Impey RW, Klein ML (1983) Comparison of simple potential functions for simulating liquid water. J Chem Phys **79**: 926–935

Liepman AH, Wilkerson CG, Keegstra K (2005) Expression of cellulose synthase-like (*Csl*) genes in insect cells reveals that *CslA* family members encode mannan synthases. Proc Natl Acad Sci USA **102**: 2221–2226

Liepman AH, Nairn CJ, Willats WGT, Sørensen I, Roberts AW, Keegstra K (2007) Functional genomic analysis supports conservation of function among cellulose synthase-like a gene family members and suggests diverse roles of mannans in plants. Plant Physiol **143**: 1881–1893

Lyczakowski JJ, Wicher KB, Terrett OM, Faria-Blanc N, Yu X, Brown D, Krogh KBRM, Dupree P, Busse-Wicher M (2017) Removal of glucuronic acid from xylan is a strategy to improve the conversion of plant biomass to sugars for bioenergy. Biotechnol Biofuels **10**: 224

Malgas S, van Dyk SJ, Pletschke BI (2015) β-mannanase (Man26A) and α-galactosidase (Aga27A) synergism - a key factor for the hydrolysis of galactomannan substrates. Enzyme Microb Technol **70**: 1–8

Martínez-Abad A, Berglund J, Toriz G, Gatenholm P, Henriksson G, Lindström M, Wohlert J, Vilaplana F (2017) Regular motifs in xylan modulate molecular flexibility and interactions with cellulose surfaces. Plant Physiol **175**: 1579–1592

Meier H, Reid J (1982) Reserve polysaccharides other than starch in higher plants. *In* **FA Loewus, W Tanner**, eds, Plant Carbohydrates I. Berlin, Springer-Verlag, pp 418–471

Moller I, Sørensen I, Bernal AJ, Blaukopf C, Lee K, Øbro J, Pettolino F, Roberts A, Mikkelsen JD, Knox JP, (2007) High-throughput mapping of cell-wall polymers within and between plants using novel microarrays. Plant J **50**: 1118–1128

Moreira LR, Filho EX (2008) An overview of mannan structure and mannan-degrading enzyme systems. Appl Microbiol Biotechnol **79**: 165–178

Nishiyama Y, Langan P, Chanzy H (2002) Crystal structure and hydrogen-bonding system in cellulose Ibeta from synchrotron X-ray and neutron fiber diffraction. J Am Chem Soc **124**: 9074–9082

Northcote D (1972) Chemistry of the plant cell wall. Annu Rev Plant Physiol **23**: 113–132

Obel N, Neumetzler L, Pauly M (2007) Hemicelluloses and cell expansion. In **J-P Verbelen, K Vissenbergm**, The Expanding Cell. Berlin, Springer-Verlag, pp 57–88

Phillips JC, Braun R, Wang W, Gumbart J, Tajkhorshid E, Villa E, Chipot C, Skeel RD, Kalé L, Schulten K (2005) Scalable molecular dynamics with NAMD. J Comput Chem **26**: 1781–1802

Piro G, Zuppa A, Dalessandro G, Northcote DH (1993) Glucomannan synthesis in pea epicotyls: the mannose and glucose transferases. Planta **190**: 206–220

Raman EP, Guvench O, MacKerell AD, Jr. (2010) CHARMM additive all-atom force field for glycosidic linkages in carbohydrates involving furanoses. J Phys Chem B **114**: 12981–12994

Reid JS, Edwards ME, Dickson CA, Scott C, Gidley MJ (2003) Tobacco transgenic lines that express fenugreek galactomannan galactosyltransferase constitutively have structurally altered galactomannans in their seed endosperm cell walls. Plant Physiol **131**: 1487–1495

Sainsbury F, Thuenemann EC, Lomonossoff GP (2009) pEAQ: versatile expression vectors for easy and quick transient expression of heterologous proteins in plants. Plant Biotechnol J **7**: 682–693

Scheller HV, Ulvskov P (2010) Hemicelluloses. Annu Rev Plant Biol **61**: 263–289

Schröder R, Nicolas P, Vincent SJ, Fischer M, Reymond S, Redgwell RJ (2001) Purification and characterisation of a galactoglucomannan from kiwifruit (Actinidia deliciosa). Carbohydr Res **331**: 291–306

Seymour GB, Colquhoun IJ, Dupont MS, Parsley KR, Selvendran RR (1990) Composition and structural features of cell-wall polysaccharides from tomato fruits. Phytochemistry **29**: 725–731

Simmons TJ, Mortimer JC, Bernardinelli OD, Pöppler AC, Brown SP, deAzevedo ER, Dupree R, Dupree P (2016) Folding of xylan onto cellulose fibrils in plant cell walls revealed by solid-state NMR. Nat Commun **7**: 13902

Sims IM, Craik DJ, Bacic A (1997) Structural characterisation of galactoglucomannan secreted by suspension-cultured cells of *Nicotiana plumbaginifolia*. Carbohydr Res **303**: 79–92

Sparkes IA, Runions J, Kearns A, Hawes C (2006) Rapid, transient expression of fluorescent fusion proteins in tobacco plants and generation of stably transformed plants. Nat Protoc **1**: 2019–2025

Stone BA, Jacobs AK, Hrmova M, Burton RA, Fincher GB (2010) Biosynthesis of plant cell wall and related polysaccharides by enzymes of the GT2 and GT48 families. In **P Ulvskov**, ed, Plant Polysaccharides: Biosynthesis and Bioengineering, Vol. 41. Oxford, Wiley-Blackwell, pp 109–165

Thomas LH, Forsyth VT, Sturcová A, Kennedy CJ, May RP, Altaner CM, Apperley DC, Wess TJ, Jarvis MC (2013) Structure of cellulose microfibrils in primary cell walls from collenchyma. Plant Physiol **161**: 465–476

Timell T (1965) Wood hemicelluloses: part II. Adv Carbohydr Chem **20**: 409–483

Tong CBS, Gross KC (1988) Glycosyl-linkage composition of tomato fruit cell-wall hemicellulosic fractions during ripening. Physiol Plant **74**: 365–370

Tryfona T, Liang HC, Kotake T, Kaneko S, Marsh J, Ichinose H, Lovegrove A, Tsumuraya Y, Shewry PR, Stephens E, (2010) Carbohydrate structural analysis of wheat flour arabinogalactan protein. Carbohydr Res **345**: 2648–2656

Tryfona T, Liang HC, Kotake T, Tsumuraya Y, Stephens E, Dupree P (2012) Structural characterization of Arabidopsis leaf arabinogalactan polysaccharides. Plant Physiol **160**: 653–666

Voiniciuc C, Schmidt MH, Berger A, Yang B, Ebert B, Scheller HV, North HM, Usadel B, Günl M (2015) MUCILAGE-RELATED10 produces galactoglucomannan that maintains pectin and cellulose architecture in Arabidopsis seed mucilage. Plant Physiol **169**: 403–420

von Freiesleben P, Spodsberg N, Blicher TH, Anderson L, Jørgensen H, Stålbrand H, Meyer AS, Krogh KB (2016) An *Aspergillus nidulans* GH26 endo-β-mannanase with a novel degradation pattern on highly substituted galactomannans. Enzyme Microb Technol **83**: 68–77

Vuttipongchaikij S, Brocklehurst D, Steele-King C, Ashford DA, Gomez LD, McQueen-Mason SJ (2012) Arabidopsis GT34 family contains five xyloglucan α-1,6-xylosyltransferases. New Phytol **195**: 585–595

Wang Y, Mortimer JC, Davis J, Dupree P, Keegstra K (2013) Identification of an additional protein involved in mannan biosynthesis. Plant J **73**: 105–117

Western TL, Skinner DJ, Haughn GW (2000) Differentiation of mucilage secretory cells of the Arabidopsis seed coat. Plant Physiol **122**: 345–356

Whitney SEC, Brigham JE, Darke AH, Reid JSG, Gidley MJ (1998) Structural aspects of the interaction of mannan-based polysaccharides with bacterial cellulose. Carbohydr Res **307**: 299–309

Willför S, Sundberg K, Tenkanen M, Holmbom B (2008) Spruce-derived mannans—A potential raw material for hydrocolloids and novel advanced natural materials. Carbohydr Polym **72**: 197–210

Yu L, Shi D, Li J, Kong Y, Yu Y, Chai G, Hu R, Wang J, Hahn MG, Zhou G (2014) CELLULOSE SYNTHASE-LIKE A2, a glucomannan synthase, is involved in maintaining adherent mucilage structure in Arabidopsis seed. Plant Physiol **164**: 1842–1856